Global morphology and physical relations between the stars, gas and dust in the disc and arms of M100

J. H. Knapen[1,2] and J.E. Beckman[3]

[1] *Department of Physical Sciences, Division of Physics and Astronomy, University of Hertfordshire, College Lane, Hatfield,*
Herts AL10 9AB, UK. E-mail knapen@star.herts.ac.uk
[2] *Département de Physique, Université de Montréal, C.P. 6128, Succursale Centre Ville, Montréal (Québec), H3C 3J7 Canada;*
and Observatoire du Mont Mégantic
[3] *Instituto de Astrofísica de Canarias, E-38200 La Laguna, Tenerife, Spain. E-mail jeb@iac.es*

ABSTRACT

We study star formation processes in the disc of the weakly barred grand design spiral galaxy M100 (NGC 4321) from a variety of images tracing recent massive star formation, old and young stars, dust, and neutral hydrogen. Differences between arm and interarm regions are specifically studied by decomposing the images into arm and non-arm zones. We find from a comparison of the morphology in Hα, H I and dust that while the first two are coincident over most of the disc, they are offset from the dust lanes especially along the inner parts of the spiral arms: a picture which is indicative of a density wave shock moving through the arms. H I is formed near the young massive stars as a result of photo-dissociation.

From radial profiles we find that in the region of the star-forming spiral arms the exponential scale lengths for Hα, blue and near-infrared light, and 21 cm radio continuum are equal within the fitting errors. The scale lengths for the interarm region are also equal for all these tracers, but the arm scale lengths are significantly longer. This points to a common origin of the profiles in star formation, with little or no influence from radial population gradients or dust in the disc of this galaxy. The longer arm scale lengths are equivalent to an outwardly increasing arm-interarm contrast. We argue that the radial profiles of radio continuum and H I, as well as CO, are also directly regulated by star formation, and discuss the possible implications of this result for the interpretation of observed CO intensities in and outside spiral arms.

We discuss the radial atomic hydrogen profile in some detail. Its almost perfectly flat shape in the region of the star-forming spiral arms may be explained by photodissociation and recombination processes in the presence of a limited quantity of interstellar dust, controlling the equilibrium between the molecular and atomic form of hydrogen. Over most of the inner part of the disc, H I seems to be a *product* of the star formation processes, rather than the *cause* of enhanced star formation.

Key words: galaxies: individual (M100, NGC 4321) — galaxies: ISM — galaxies: photometry — galaxies: spiral — galaxies: structure — radio lines: galaxies

1 INTRODUCTION

In order to learn more about the interaction between the different components of the ISM and about the processes leading to star formation (SF) in the arms of spiral galaxies, it is important to compare directly arm regions with those between the arms (interarm regions). So far, only a limited number of grand-design, late-type spiral galaxies has been studied in detail in this sense combining information from several tracers of SF and neutral gas throughout their discs.

This is because the resolution attainable with radio and millimeter observations entails the selection of galaxies with large angular size, which implies long mapping times. For both interferometric observations of H I and single-dish CO measurements the limiting angular resolution is around 15″, corresponding to slightly over 1 kpc in the case of NGC 4321, the relatively nearby Virgo spiral studied in the present paper. Given that the scale of the spiral arms is typically also some 1 kpc, galaxies at larger distances are not suitable for this kind of study.

Comparing arm with interarm regions, Cepa & Beckman (1990) found for NGC 628 and NGC 3992 that the Hα/H$\,$I ratios were higher in the arms than between them, and that the arm/interarm ratios of Hα/H$\,$I vary congruently along the two main arms. They interpreted the pattern in the arm/interarm ratios as indicating the locations of the density wave resonances, and were able to determine a pattern speed in that way. Tacconi & Young (1990) found an enhanced Hα to CO ratio in the northeast arm of NGC 6946 as compared to the neighbouring interarm region, implying triggering of the star formation in the arm if the CO reliably traces the molecular gas mass, but the southwest arm of that galaxy does not show such an enhanced Hα/CO ratio.

The galaxy M51 has received quite a lot of attention in this respect. Lord & Young (1990) studied arm and interarm regions separately using CO and Hα data, but they were limited to the 45$''$ resolution of their CO data which was not quite adequate to isolate the spiral arms. Knapen et al. (1992) combined the Nobeyama CO map from Nakai et al. (1991; see also Nakai et al. 1994) with H$\,$I and Hα data to determine the arm-interarm ratio of the massive star formation efficiency, defined as Hα luminosity per unit total (atomic plus molecular) gas. They found a pattern of dips and strong peaks in the arm-interarm efficiency ratio, which is symmetric in the two main arms of M51. The fact that the efficiency ratios are consistently larger than unity along both arms is strong evidence for triggering of the massive SF in the spiral arms. García-Burillo, Guélin & Cernicharo (1993), using IRAM CO data of slightly higher resolution than those used by Knapen et al. (1992), confirmed the findings of the latter authors on relative arm/interarm contrasts. For the galaxy studied in this paper, NGC 4321, Knapen et al. (1996), using new CO data from Nobeyama (see also Cepa et al. 1992) and combining it with Hα and H$\,$I maps, found that the massive SF efficiencies are enhanced in the arms with respect to the interarm regions. The arm/interarm efficiency ratios are very similar to those found by Knapen et al. (1992) in M51, but the symmetric pattern of peaks and dips so obvious in M51 is absent from NGC 4321. Knapen et al. (1996) argue that their conclusion on triggering can only be strengthened if possible arm/interarm variations in dust extinction or the CO to H$_2$ conversion factor are considered.

In the present paper, we will discuss the spatial relationships between not only CO, H$\,$I, and Hα, but also blue and near-infrared (NIR) light, and radio continuum. We will do this via direct 2-dimensional comparison of some tracers, and through a comparison of radial (azimuthally averaged) profiles. Similar profiles for a number of tracers have been discussed by (among others) Tacconi & Young (1986) for NGC 6946 and Rand, Kulkarni & Rice (1992) for M51, but nowhere in the literature has the specific difference between arm and interarm environments been taken into account when studying radial profiles. Apart from whole disc radial profiles, here we also study radial profiles for the arm and interarm zones separately.

NGC 4321 (M100) is a weakly barred spiral galaxy with two main spiral arms. It hosts a circumnuclear starburst region in its central region, which has been studied extensively by Knapen et al. (1995a,b). In this paper, we will concentrate on a region between some 30$''$ and 250$''$ in radius (or $0.1(D_{25})/2 < R < 1.2(D_{25}/2)$) comprised of part of the bar, and the disc of the galaxy. The bar (Pierce 1986; Knapen et al. 1993) extends to some 60$''$ in radius. We assume a distance to NGC 4321 of 17.1 Mpc (Freedman et al. 1994), thus 12$''$ corresponds to 1 kpc.

We define here as the "north arm" the arm originating at the end of the bar east of the nucleus, passing north of the centre and continuing toward the west and south-west. The arm we denominate as the "south arm" starts west of the nucleus at the end of the bar, passes south of the central region, and continues toward the east and north-east.

After a short description of the observational data used (Section 2), we discuss the spatial correlation of radio and optical emission in Sect. 3. In Sect. 4 we present radial profiles for the whole disc of the galaxy, but also for arm and interarm zones separately, and compare exponential scale lengths fitted to the radial distributions. We discuss the results critically in terms of star formation processes in Sect. 5, with a specific discussion of the origin and role of H$\,$I in Sect. 6. We briefly summarize the main conclusions in Sect. 7.

2   OBSERVATIONAL MATERIAL

In the present paper, we use data on NGC 4321 from our own published research papers. In this Section, they will be reviewed only very briefly, since more technical details can be found in the original studies. The radio data used are from Knapen et al. (1993): an H$\,$I map of the whole galaxy at 15$''$ resolution obtained by moment analysis from a uniformly weighted VLA data cube; and a 21cm radio continuum image (also at 15$''$ resolution), which is the map that was subtracted from the individual channel maps in order to produce the H$\,$I line data-set. The Hα image of the disc of NGC 4321 was shown also by Knapen et al. (1993), and a detailed study of the statistics of the H$\,$II regions throughout the disc can be found in Knapen (1996). Here we start out with a slightly smoothed version of the original image (with a resolution of 2$''$), but we will also use a further smoothed version with resolution 15$''$, in order to compare directly with the H$\,$I data. Pixel sizes of the original; 2$''$; and 15$''$ resolution images are 0.$''$27; 0.$''$54; and 2.$''$0, respectively. The B and I images used here (also shown by Knapen et al. 1993) are discussed in more detail by Beckman et al. (1996). A $B-I$ colour index image was produced by dividing one image by the other. Since the central $\sim 10''$ part of the I band image is saturated, the $B - I$ image is not reliable in this inner region. A $B-I$ image shows both effects due to changing stellar populations and localized extinction by dust, two effects that can be relatively well separated morphologically on a map, but less easily when studying integrated emission (such as in radial profiles). The total field of view of all the images used contains the complete disc of NGC 4321, out to $> (D_{25}/2)$. All images were given a common orientation using the position of the centre of the galaxy and those of stars in the field. Finally, we refer to single dish CO measurements of a number of points in the disc of NGC 4321, and mostly along the inner parts of the two main spiral arms (Cepa et al. 1992; Knapen et al. 1996).
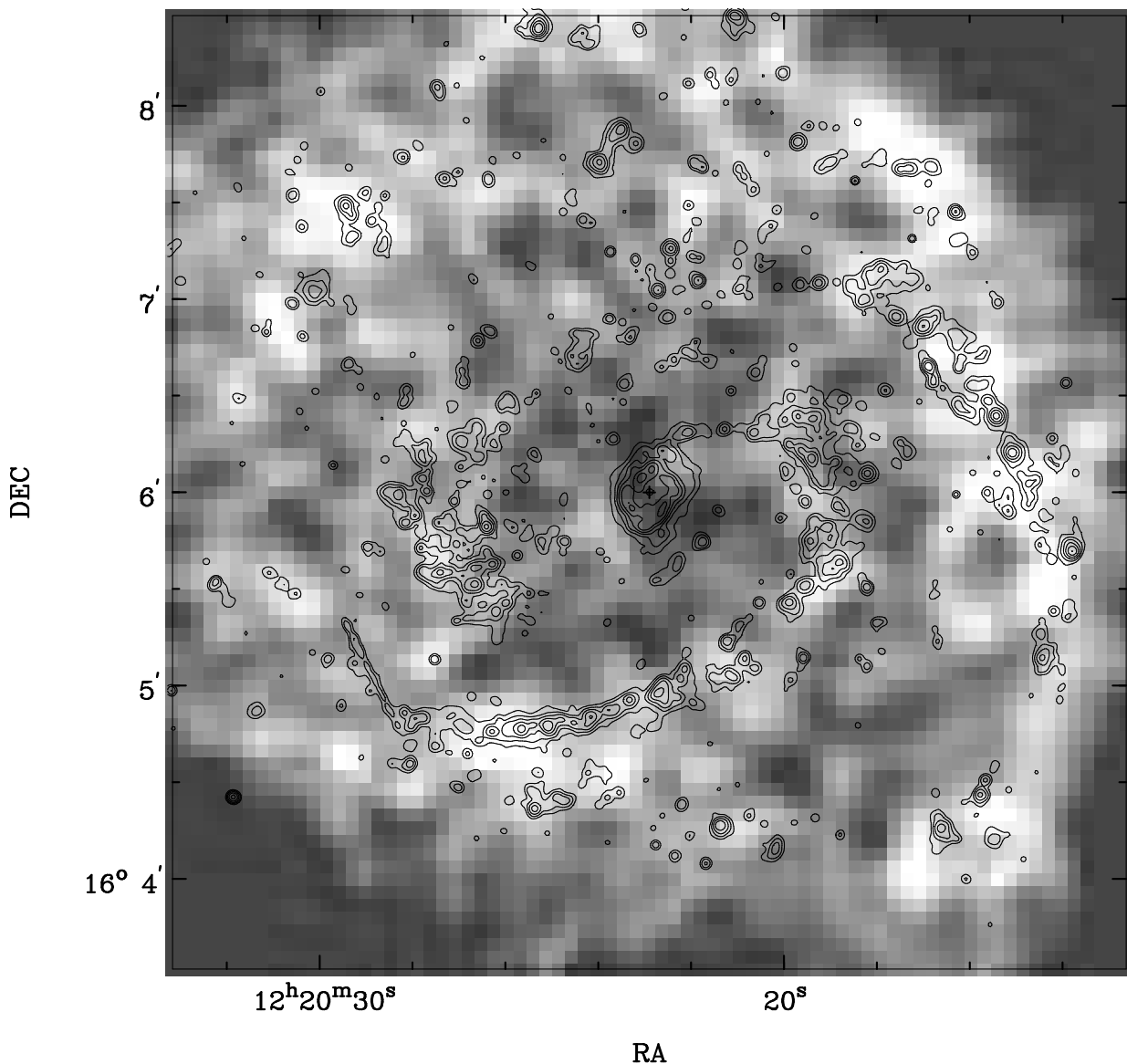
Figure 1. (*a*) Overlay of the 2″ resolution continuum-subtracted Hα image of NGC 4321 (contours) on a grey-scale representation of the H I total intensity map at 15″ resolution. Contour levels are 0.37, 0.74, 1.48, 2.95, 5.90, 11.8, and 23.6×10^{36} erg s^{-1}. Greys are from 0.98 to 14.7×10^{20} atoms cm^{-2}.

3 SPATIAL (ANTI-)CORRELATION OF DIFFERENT TRACERS

In order to study the relative location of dust, young stars, and atomic hydrogen, we present overlays of Hα (which traces young massive stars) on H I (atomic hydrogen) (Fig. 1 a,b), Hα on $B - I$ (indicating the location of the dust lanes; Fig. 2), and H I on $B - I$ (Fig. 3). We will compare these with overlays of interferometric CO observations (Rand 1995) on some of the images also used in the present paper, especially Rand's Fig. 2 showing CO on our Hα and $B - I$ in a selected region W and S of the nucleus.

Fig 1a shows the Hα at high resolution overlaid on H I, while in Fig. 1b the smoothed Hα image (15″ resolu-

tion) is overlaid on the H I image of the same resolution. The morphology of the disc of NGC 4321 is apparent from the Hα. The strong Hα emission of the central region is in fact organized in a two-armed mini-spiral (see Knapen et al. 1995a,b for a detailed discussion). The weak stellar bar (Pierce 1986; Knapen et al. 1993) extends to some 40″ in radius, and does not show much Hα emission. The main spiral arms are well defined in Hα outside two strongly emitting regions at the ends of the bar. Although the general arm shape is that of a two-armed grand design galaxy with two symmetric spiral arms, the Hα distribution along the arms outside the SF regions at the ends of the bar, is in fact anti-symmetric. Along the south arm, Hα emission is strong in the region parallel to and south of the bar, whereas there

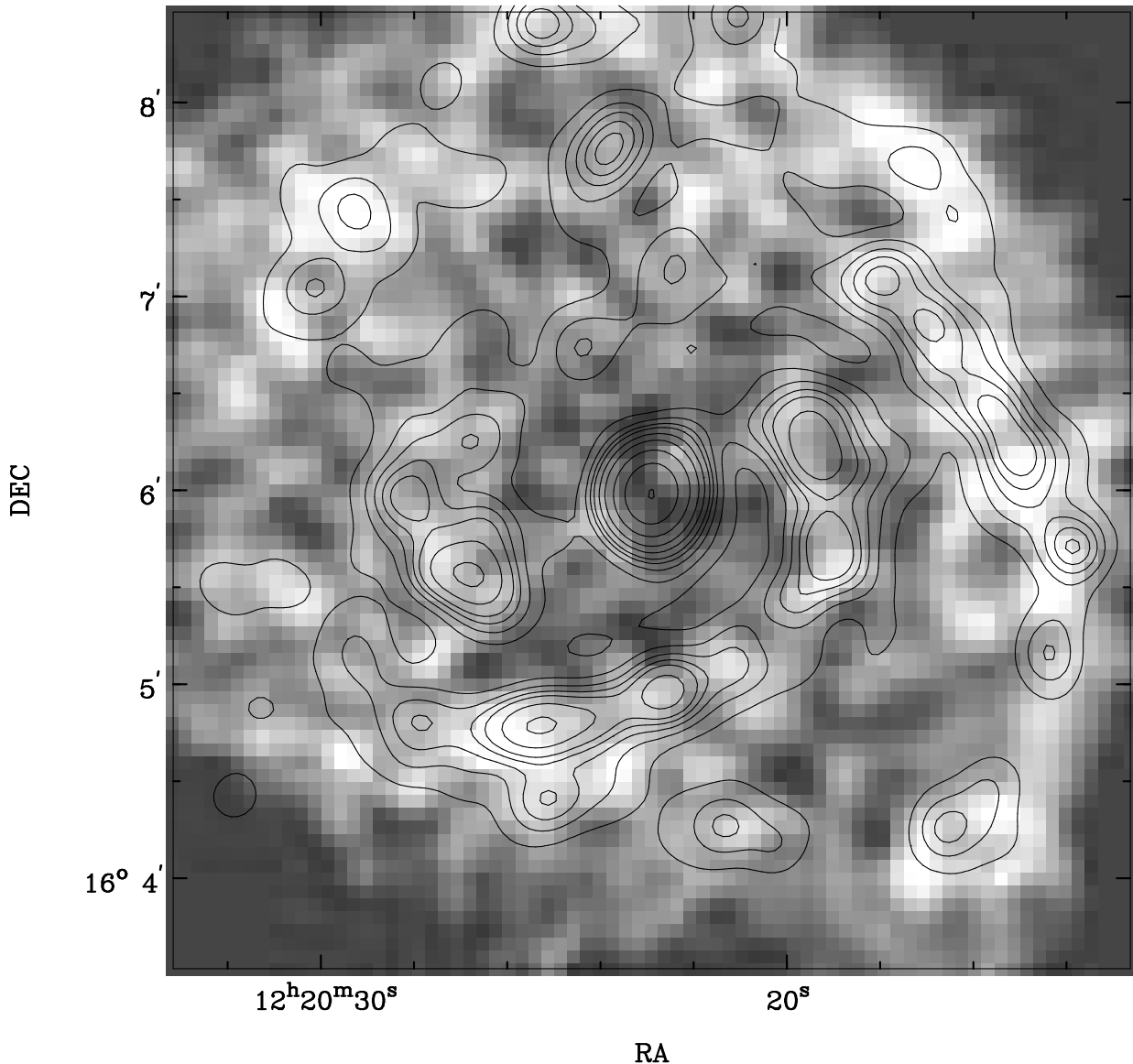**Figure 1.** (*b*) As Fig. 1a, but now a smoothed version (at 15″ resolution) of the Hα image is shown overlaid. Contour levels are 0.12, 0.25, 0.37, 0.49, 0.62, 0.86, 1.23, 1.97, 3.20, and 4.92×10^{36} erg s^{-1}.

is considerably less Hα emission along the north arm parallel to the bar (see Knapen et al. 1996 for a discussion of SF and efficiencies along these arm segments). Further along the arms, the Hα emission picks up along the north arm (near $\alpha = 12^{\mathrm{h}} 20^{\mathrm{m}} 18^{\mathrm{s}}$, $\delta = 16°7'$) but almost completely disappears in the other arm ($\alpha = 12^{\mathrm{h}} 20^{\mathrm{m}} 28^{\mathrm{s}}$, $\delta = 16°5'$). The strong Hα emission along the north arm stops near $R \sim 120''$ (near $\alpha = 12^{\mathrm{h}} 20^{\mathrm{m}} 15^{\mathrm{s}}$, $\delta = 16°6'$), and outside that radius the Hα emission along both arms is weak and not continuous, although still outlining the spiral arms (see also the next section). Interarm Hα emission is present in large portions of the disc, but is usually weak, and arises from small, isolated regions, which in some cases are however lined up along spiral arm fragments.

3.1   H I and Hα

From both Fig. 1a and b it is clear that along the two main spiral arms, the Hα emission generally coincides with the H I. The H I emission is depressed in the circumnuclear and bar regions, and is not very strong along the north arm segment parallel to the bar. But especially along the arm segments south and west of the nucleus, where the Hα is strong and defines the arm shape, the H I coincides well with the Hα. From Fig. 1b it is clear that most regions emitting strongly in H I (white in the grey-scale Figure) are accompanied by a patch of Hα emission. This is even more evident from the high resolution Hα overlay (Fig. 1a), which shows that practically all regions of H I emission are accompanied by one or more H II regions emitting in Hα. Since many small

Figure 2. The $2''$ Hα image from Fig. 1a shown overlaid on a grey-scale representation of the $B-I$ colour image of the disc of NGC 4321. Redder colours (e.g. dust lanes) are represented by darker shades, bluer colours (e.g. sites of recent or ongoing SF) by lighter shades. Greys range from 0.7 mag (white) to 2.4 mag (black). Contours as in Fig. 1. Note that the $B-I$ image cannot be used at those pixel positions where the I image was saturated (mostly in the nuclear region). These pixel values were discarded and show up black in the Figure.

H II regions are scattered over most of the disc surface, it is important to note that most dark spots (no, or reduced, H I emission) in the figure are *not* accompanied by any Hα emission. We thus find that along most of the spiral arms, and certainly where the arms are well defined and strong in Hα, the H I and Hα emission spatially coincide, but also that individual patches of H I emission over the whole disc surface are generally accompanied by Hα emission.

3.2 Dust lanes

Fig. 2 shows an overlay of the Hα image on the $B-I$ colour index map. Although in a $B-I$ image alone the detailed effects due to extinction by dust and changing stellar populations (which can both result in a redder colour) cannot be distinguished, the $B-I$ image does indicate the location of the major dust lanes in the disc of the galaxy. When compared with the true-colour image of NGC 4321 presented by Beckman et al. (1996; see also Peletier 1994), it is evident that the dark lanes along the arms and in the central (bar) and interarm regions are in fact dust lanes, as is also indicated by their characteristic patchy appearance.

Fig. 2 shows that the Hα emission is generally offset from the dust lanes, in the spiral arms, in the bar, and in some cases also in the interarm region (see e.g. the region east of the bar). This picture is indicative of the presence of a density wave pattern in which the dust lanes indicate the gas compression zone, and the Hα results from young stars being formed just downstream from there (the North side of the galaxy is the approaching side [Knapen et al. 1993], thus the downstream side of the arm in this region which is inside corotation [e.g. Knapen et al. 1996] is the convex side). This is seen especially clearly along the first $\sim 90°$ in PA of the south arm, starting immediately outside the circumnuclear zone, and also along most of the north arm. The shape of the dust lanes in the bar zone is indicative of streaming due to a weak bar (Athanassoula 1992); the lanes are accompanied by a string of H II regions (see also Knapen et al. 1995b).

Along the part of the south arm immediately south of the centre, the situation is not quite as clear. The dust lane bifurcates, and in fact surrounds the Hα emission in this part of the arm, although the stronger lane remains on the concave side of the Hα arm. In the outer part of the disc ($R > 120''$), where the arms are not well defined in Hα, dust lanes are hardly visible and the situation is much less clear.

Fig. 3 shows graphically what can in principle be de-

Figure 3. The H I image from Fig. 1, now in contour representation, shown overlaid on the $B - I$ colour image of Fig. 2. Greys as in Fig. 2. H I contours are from 4.88 to 14.7 in steps of 1.95×10^{20} atoms cm^{-2}. Note that lower H I contours have been emitted for clarity from this Figure (compare with Knapen et al. 1993).

duced from Figs. 1 and 2: that the H I is generally offset from the dust lanes, and coincides with the SF regions, which have blue colours in $B - I$. The general offset between dust lanes and H I spiral arms is particularly clear from this overlay. Many of the regions where H I and Hα emission coincide, as discussed above from Fig. 1, can be recognized.

3.3   CO

Rand (1995) presented overlays of his new BIMA interferometric CO image on the same Hα and $B - I$ images as used in the present paper. His CO data cover the south arm only up to where the strong Hα complex ends. Rand finds that in the bar and along the first part of the arm, the CO coincides with the dust lanes, and is offset from the Hα. He interprets the behaviour in the bar and along the inner part of the arm as an indication that the star formation is triggered by gas compression within the bar potential, and by the density wave, respectively. Further along the arm, where the dust lane bifurcates, the CO emission coincides with the Hα, and not with the dust lanes. According to Rand, this zone may be close to corotation (where no offset is expected between stars and the dense gas from which they form), but the dust lanes may trace diffuse gas that has little to do with SF. An alternative explanation would be that the CO does not trace the molecular hydrogen, but is in fact seen

where it is heated by the SF activity (see below). Comparison of the relative locations of this arm segment in CO and (non-thermal) radio continuum could shed light on the importance of cosmic-ray heating of the CO (cf. Adler, Allen & Lo 1991; Allen 1992), but unfortunately the 21 cm map used here is not of sufficient quality to use in this sense.

4   RADIAL PROFILES

4.1   Whole-disc profiles

Radial profiles of several gas and stellar tracers are shown in Fig. 4. All curves are azimuthally averaged radial profiles, made by integrating in elliptical annuli, all centred on the nucleus of the galaxy. We assumed values of $i = 27°$ for the inclination angle of the galaxy, and PA$= 153°$ for the position angle of the major axis (Knapen et al. 1993); these values were kept constant for all ellipses. Except for the high-resolution Hα profile for which we used $2''$ ellipses and spacings, all profiles were calculated integrating in $10''$ wide ellipses, with radii also increasing by $10''$ per step. In Hα we determined profiles at two different resolutions: one with the same resolution as the radio data ($15''$, from a smoothed Hα image), the other at $2''$ resolution. Apart from the inner region ($r_D < 30''$) there are no differences between the two
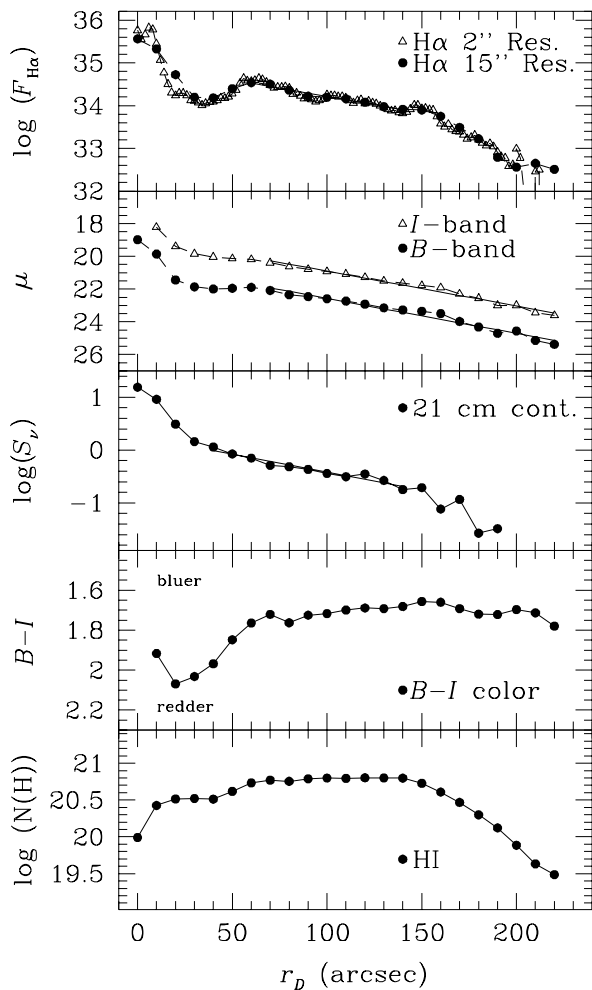
Figure 4. Azimuthally averaged radial profiles of Hα at 2″ (open triangles) and 15″ (filled dots) resolution (upper panel); B (blue; filled dots) and I bands (NIR; open triangles) (second panel); 21 cm radio continuum (third panel); $B - I$ colour (fourth panel); and 21 cm H I (lower panel). Drawn lines indicate exponential fits to the data points; fits were made in the ranges where the lines are drawn. Units are log of erg s^{-1} arcsec^{-2} for Hα, magnitudes for B and I bands, log of mJy/beam for 21cm continuum, magnitudes for $B - I$, and log of atoms cm^{-2} arcsec^{-2} for H I.

Hα profiles which might influence the interpretation or the fitting of scale lengths, so we feel confident in using profiles determined from images (not only in Hα) at resolutions of around 15″ for the analysis below.

Other profiles plotted in Fig. 4 represent the distributions of blue and red light (B and I bands); 21 cm radio continuum; $B - I$ colour index; and 21 cm H I. Note that all quantities are plotted either on a magnitude or purely logarithmic scale, so that exponential profiles appear as straight lines in the figure.

Some of the most important characteristics of the morphology of NGC 4321 can be recognized in the radial profiles, most easily so in the Hα. The nuclear region extends to about 15″ and emits strongly in Hα (Knapen et al. 1995a,b). The radial Hα profile is sharply peaked here ($0″ < r_D < 15″$). The region of the (weak) bar, with low Hα emission, extents from some 15″ to 40″ in radius. Two

Table 1. Exponential scale lengths (h, in arcsec) for different tracers (Hα at 15″ resolution, B, I and 21cm continuum) for the disc of NGC 4321, as well as for the arm and interarm zones separately.

h (″)	Disc	Arm	Interarm
Hα	55.4±3	85.9±3	61.1±3
B	50.7±3	79.3±3	55.5±3
I	50.9±3	77.6±3	54.3±3
21cm cont.	63.7±6	81.4±7	60.1±6

regions of enhanced SF at the ends of the bar show up as a bump around $r_D = 60″$, followed by a region where the Hα luminosity falls off exponentially, which is where the SF spiral arms in the disc of NGC 4321 are found. After a break in the profile at $r_D \sim 140″$, the profile falls off rapidly. The Hα disc ends near $r_D = 200″$, or $0.95\,(D_{25}/2)$.

The specific zones seen in the Hα profile can be recognized in the B and I profiles: a central peak, a depression in the bar region (less pronounced in I, as expected for an older, redder, bar population), and enhanced emission from the region of the SF spiral arms (though less enhanced than in Hα). The radio continuum profile also shows the central peak, followed by an exponential decline, not very different from the optical profiles. The $B - I$ colour profile is notable in that it is practically constant, after a blue peak due to the SF in the central region and a red depression in the bar zone. The H I profile is the only one not showing a central peak, and in fact the main resemblance it shows to the other profiles is that it is slightly enhanced between $60″ < r_D < 140″$, or exactly in the region defined above as the SF spiral arm domain.

We fitted exponential scale lengths h to the radial profiles in the region of the SF spiral arms ($60″ < r_D < 150″$) by least squares fits to the data points. The results and their estimated uncertainties are listed in Table 1, and the fits are indicated as continuous lines in Fig. 4, where the extent of the line shows the exact range in radius used for fitting in each case. The main result is that scale lengths for Hα, B and I do not differ significantly, whereas the radio continuum scale length is marginally longer than the optical one, but is within 1σ of $h_{Hα}$. Note that larger scale lengths in radio continuum could be expected because of cosmic ray propagation (e.g. Helou & Bicay 1993). The Hα and optical scale lengths are also very similar to the scale length determined for the CO distribution[⋆] ($h_{CO} = 46 \pm 8″$, Kenney & Young 1988; Knapen et al. 1996). The optical values agree with Grosbøl's (1985) value of $48″.9$, but differ from the values found by Elmegreen & Elmegreen (1984) of $h_B = 71″.2$ and $h_I = 69″.1$. Such a difference may be due to different ranges used for the fits (see Knapen & van der Kruit 1991). Note that Beckman et al. (1996) find slightly different values for the scale lengths but these differences may well be

---

[⋆] Note that the CO scale length was not obtained from an azimuthally averaged radial profile, but from observed points in the disc, which may be biased toward points on the spiral arms. In using the CO scale length as we have done here, one assumes that no changes with radius of azimuthal variations in CO emission are present. The large error bars on h_{CO} reflect this.
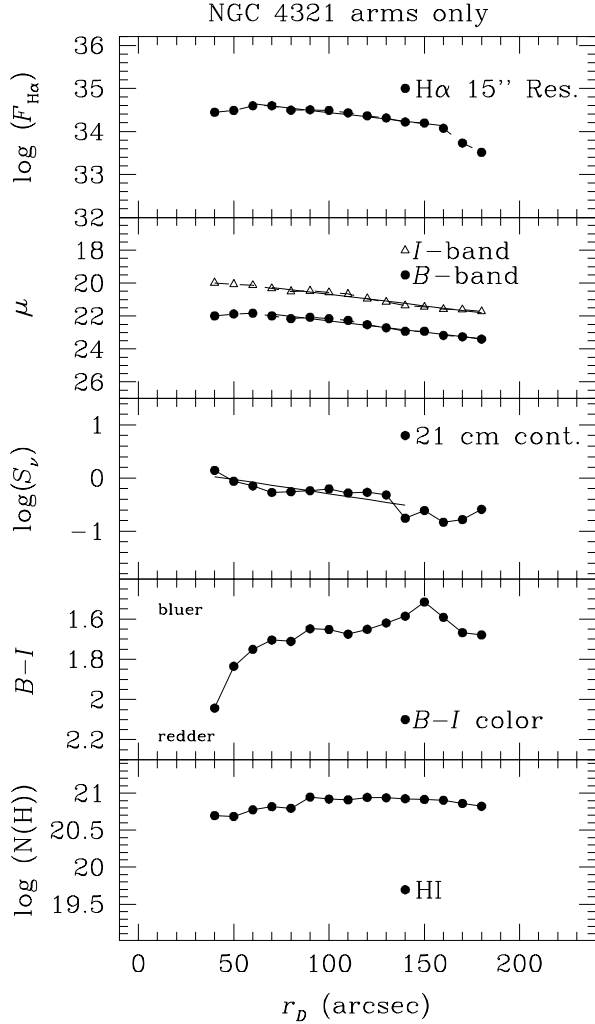
Figure 6. As Fig. 4, now for arms (a.) and interarm regions (b.) separately.

Figure 6. (*b*)

due to the fact that they did not fix the position angle and inclination in the fits, along with different definition of arms and interarm regions. Ryder & Dopita (1994) found that the Hα scale lengths for a sample of 34 nearby southern spirals were in general larger (but smaller or equal in about 1/5 of the cases) than those in V and I. Where the Hα scale lengths are longer, they find that the V scale lengths are usually also longer than those in I. However, NGC 4321 was not included in their sample, and since no unique general rule about the Hα versus V scale length behaviour can be inferred from their work, it is hard to comment further. We conclude that, within the uncertainties, disc scale lengths for NGC 4321 in Hα, B, I, 21cm continuum and CO are equal, with $h_\mathrm{d} = 53'' \pm 2''$.

4.2   Separate arm and interarm radial profiles

The similar scale lengths for optical, Hα, radio continuum and CO emission point strongly toward a common origin. To test this in more detail, we produced separate arm and interarm images for all tracers, except CO where no complete
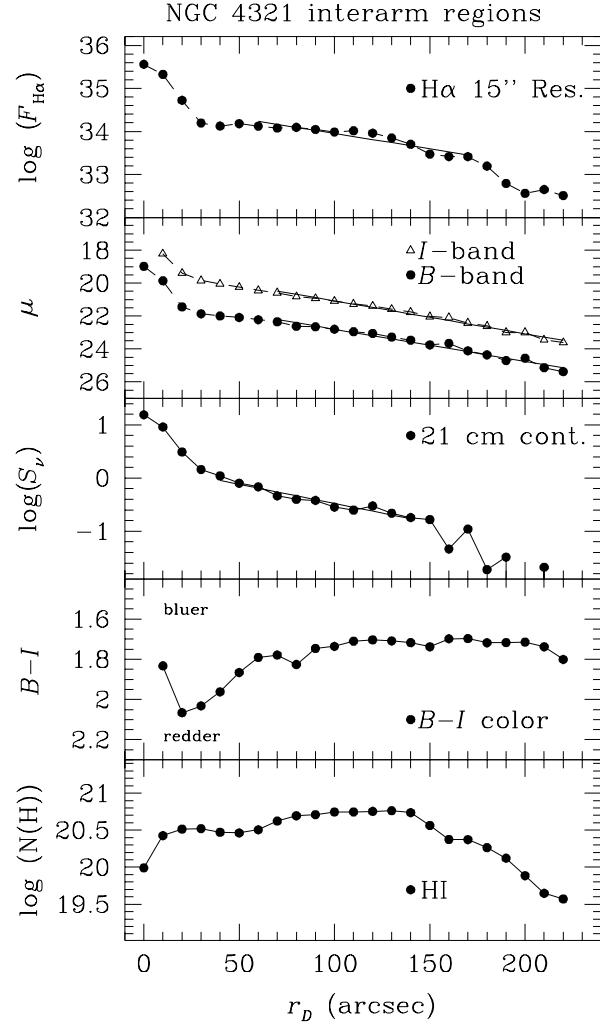
map of NGC 4321 is available. The Hα image was used to identify the spiral arms, which were outlined interactively. A mask image was produced that was combined with the Hα, B, I, radio continuum, $B - I$ and H I images to make the separate arm and interarm maps for all tracers. The outline of the adopted spiral arm region is shown overlaid on the Hα image in Fig. 5. Following the ellipse fitting procedure described above for the whole disc profiles (hereafter "disc profiles"), we produced separate arm and interarm radial profiles and fitted exponential scale lengths (Fig. 6a,b; Table 1).

The interarm profiles and scale lengths look similar to those found for the disc, which reflects the fact that most of the disc area is in the interarm regions, whereas only a relatively small area can be defined as arms. Interarm scale lengths in Hα, B, I and 21cm continuum are equal within the uncertainties of the fit, even though in most cases they are somewhat larger than those for the disc ($h_\mathrm{ia} = 56'' \pm 3''$). Although counterintuitive, the disc scale length can be somewhat smaller than both the interarm and arm scale lengths due to the outward decrease of the relative number of arm pixels. The arm profiles are in all cases flatter than
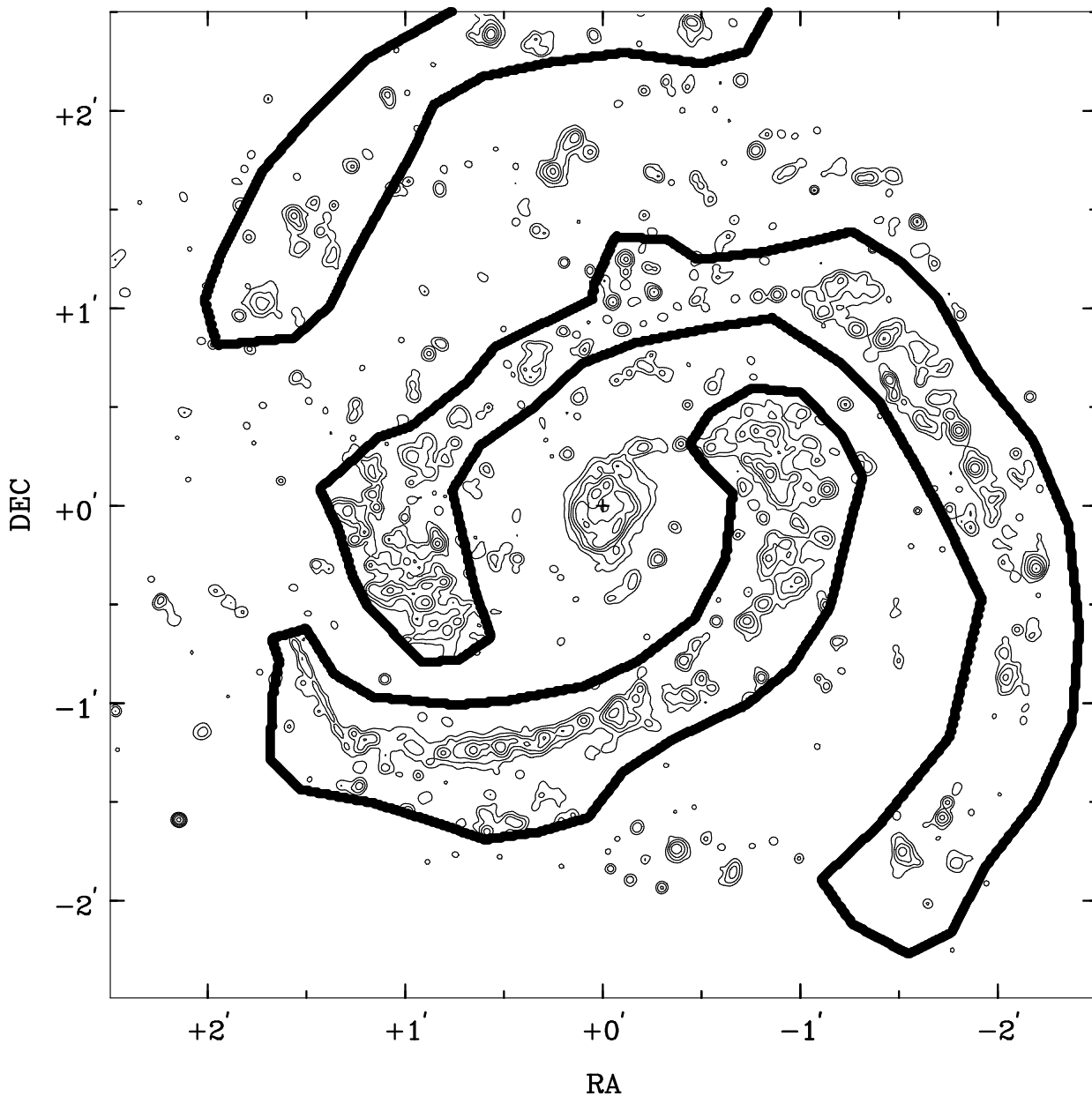
Figure 5. Outlines of the mask used to separate arm from interarm regions (heavy contour) overlaid on a contour representation of the 2″ resolution Hα image of Fig. 1a. Hα contours as in Fig. 1a.

the disc and interarm profiles, except for $B - I$ which is slightly rising. The arm scale length values reflect the flat profiles: they are more than 50% larger than those for the disc. It is remarkable that arm scale lengths in Hα, B, I and radio continuum are again practically the same, around $h_a = 81'' \pm 3''$.

The longer arm scale length can be interpreted as a direct effect of enhanced SF in the arms, and is equivalent to the observation that the arm-interarm contrast rises radially outward (where this contrast is defined as the ratio of average arm intensity to average interarm intensity). Similar results were found earlier, using different techniques,

by Schweizer (1976) for 6 spiral galaxies, and by Carignan (1985) who considered blue and red pixels separately for 3 late-type spirals. The fact that the values for optical, Hα and radio continuum emission (and CO for the disc) are equal in NGC 4321 implies that all these tracers are directly related to the SF activity. We will discuss these results, their validity and their implications in more detail below.

5 STAR FORMATION IN DISCS OF SPIRAL GALAXIES

In Sect. 4.1 we saw that the radial fall-off in the disc of NGC 4321 is very similar for $H\alpha$, B, I, radio continuum, and CO, with equal exponential scale lengths for all tracers. The H I and the $B - I$ colour profiles show a distinctly different behavior. A similar picture is seen in the galaxies NGC 6946 (Tacconi & Young 1986) and M51 (Rand et al. 1992), where the $H\alpha$ and CO (and in the first case also blue light and radio continuum) decline together, whereas the H I shows a depression in the centre, and joins the other profiles only in the outer parts of the disc.

In the present paper we have gone one step further and decomposed the profiles into arm and interarm contributions. Whereas the scale lengths in the arms and those in the interarm regions are significantly different, the separate tracers: $H\alpha$, B, I, and radio continuum, still have one common scale length in the arms, and another in the interarm regions. We will now discuss these results considering several mechanisms that can affect them.

5.1 Dust

First we must consider the effect of dust extinction and absorption on the scale lengths as determined in the optical. Assuming that the amount of dust in a galactic disc declines radially (which happens naturally if dust and stars are uniformly mixed), this will lead to increasingly longer scale lengths toward the blue (Evans 1994; de Jong 1995; Peletier et al. 1995; Beckman et al. 1996). This is in fact observed to varying degrees in other galaxies studied, indicating varying amounts of dust in the disc. But in NGC 4321 we find equal scale lengths in blue and NIR, although the arm scale lengths are longer than the ones in the interarm regions. For NGC 4321, Beckman et al. (1996) claim that most of the disc is largely dust free, and explain the seemingly contradictory observations of many well-developed dust lanes in optical and colour images by the confinement of the dust to these relatively narrow lanes so the effect on the disc as a whole is small. Note that according to Beckman et al. (1996) the other two galaxies they studied, M51 and NGC 3631, and for which they did find longer scale lengths toward shorter wavelengths, do contain significant quantities of dust distributed in the disc.

The considerations of Beckman et al., and the fact that the scale lengths in blue and NIR light, but also in $H\alpha$ and radio continuum, behave so similarly must lead to the conclusion that the disc of NGC 4321 is indeed largely dust-free, and that the difference between arm and interarm profiles cannot be a result of arm-interarm variations in dust extinction. The dust visible as the dust lanes, e.g. in Fig. 2, is mostly confined to those dust lanes, with the $H\alpha$ emitting regions aligned with the dust lanes but always offset from them. The fact that the B and I profiles are so similar in the disc (also directly indicated by the nearly flat $B - I$ profile), and separately in the arms and interarm regions as well, indicates that radial population gradients must be very small. If such gradients do exist, dust extinction must exactly cancel their effects on the radial profiles. This would amount to a conspiracy which we prefer to reject.

In fact we can go some way to setting quantitative lim-its on the dust content if we assume that all the components of the arms, or of the interarm disc, have the same geometrical (exponential) radial distribution. Taking this assumption, a formula by Regan & Vogel (1994) can be used to relate the on-axis, or equivalent face-on, extinction at a given wavelength to the ratio of the measured scale length at that wavelength and the true scale length: the formula referred to is their equation (12). We take the maximum permitted differences between the measured B and I scale lengths, using the errors quoted in Sect. 4, to obtain upper limits to the effective mean dust content. In both the arms and the interarm disc the on-axis dust extinction estimated in this way must be less than 0.1 mag. However, as Beckman et al. (1996) point out, an extinction of 0.1 mag obtained this way can be reproduced by a dust lane of on-axis optical depth 1 but covering only 10% of the system (arm or interarm disc) as seen face-on. In fact the presence of dust lanes or patches with much greater optical depths could be missed in the above estimates, provided that they cover only a moderate fraction of the face-on disc. Thus our conclusion here is that the effective global extinction over the arms or the interarm disc, must be low, but the present results do not preclude the presence of non-uniform dust, compressed either in lanes or into the plane of the galaxy, or both.

5.2 Star Formation

The four main sections of the $H\alpha$ profile (central peak, dip in bar region, exponential decline, and steeper decline after $R = 160''$) can be recognized in the $H\alpha$ image (Fig. 1). Enhanced SF in the central region and in the main spiral arms between $50'' < R < 160''$ causes the relatively enhanced region in the radial profile, whereas the lack of SF in the bar region coincides with the depression in the radial profile. The part of the profile where we determined the exponential scale lengths coincides with the region where the star-forming spiral arms are found, and it is tempting to conclude that not only the $H\alpha$ profile is controlled by SF, but also, since the scale lengths are equal, the B and I, radio continuum and CO profiles (like in NGC 6946, Tacconi & Young 1986).

This is confirmed by considering the separate arm-interarm profiles. Having noted (in the previous Section) that dust extinction is not varying significantly between the arms and the interarm regions, the most important ground for difference between the arm and interarm results is in the rate of SF. If indeed the SF activity is the underlying cause for the equal scale lengths for different tracers in the disc as a whole, one might expect differences in arm and interarm behaviour, congruent in all tracers, and showing more SF in the arms. This is exactly what the disc profiles, as well as the separate arm and interarm profiles show. We conclude that the differences between arms and interarm scale lengths, as well as the equal scale lengths for $H\alpha$, B, I and 21cm continuum in both the arm and interarm regions separately, are due exclusively to enhanced SF activity in the arms, and not (for example) to differential dust extinction. This is in accord with the conclusions reached by Knapen et al. (1996), who find that the massive SF rates but also efficiencies are

at least some 2 or 3 times higher[†] in the arms compared to the regions outside the arms. Since much of the I-band light may well be from the old disc, and not from recent SF activity, this would imply also that the SF rate has not changed overall in the disc over a substantial timescale. This would not be unusual, since in many galaxies old and young discs have about the same intrinsic scale length, apparent differences being due to dust (e.g. Peletier et al. 1995; Regan & Vogel 1995).

5.3   Radio continuum and CO

Young & Scoville (1982) found that in NGC 6946 the CO radial profile followed the blue light distribution. Combining Young & Scoville's data with Hα imaging, DeGioia-Eastwood et al. (1984) suggested that the SF efficiency (SF rate per unit H_2 surface density) is constant with radius. For NGC 4321, we also find that the radial CO distribution follows those of blue light and Hα. If the CO intensity is proportional to the molecular gas density, this indeed means that the massive SF efficiency does not vary radially in the disc.

A 21 cm radio continuum map, such as the one used in the present paper, reflects a combination of thermal emission (mostly from ionized gas in H II regions) and non-thermal synchrotron emission (from relativistic electrons in supernova remnants, and in the galactic magnetic field). Although we lack spectral index information needed to separate thermal from non-thermal emission, it is interesting to see that the radial profiles for the disc, but also for the arm and interarm zones, have the same scale lengths as the optical tracers. In analogy with M51, we may expect that also in M100 the non-thermal component is most likely to be stronger than the thermal one (Tilanus et al. 1988 find that in M51 only some 5% of the radio emission at 20 cm is thermal).

Since in the case of NGC 4321 both H II regions (observed via Hα emission), young stars (via B) and old stars (I) behave very similarly radially, it is not surprising that also the radio continuum shows similar scale lengths in the radial distribution. This does, however, confirm our conclusion that dust extinction cannot play an important role in the disc of NGC 4321. If it did, blue light and Hα emission should be especially affected, but the radio continuum would remain unchanged. Again, a special distribution of stars might counteract the effects of dust, but this precise numerical cancellation would be a "conspiracy".

Whereas a discussion of the detailed relation between stellar emission, the ISM, and the non-thermal radio continuum is outside the scope of this paper, we remark that the radio continuum is some measure of the cosmic-ray density throughout the disc. This has been discussed in some detail by Adler et al. (1991) and Allen (1992), who find that the ratio of velocity-integrated CO emission and non-thermal radio continuum brightness shows a remarkably small range within some large spiral galaxies, but also among them.

[†] This is a lower limit to the true efficiency ratio if the CO intensity is controlled not only by the quantity of molecular hydrogen but also by SF through e.g. enhanced FUV flux, metallicity or cosmic-ray density, resulting in more "hidden" neutral gas in the interarm regions.

This could imply that the CO intensity is controlled by the UV flux and the cosmic ray density, more than by the column density of molecular hydrogen (Allen 1992), as also discussed by Rubio, Lequeux & Boulanger (1993), Lequeux et al. (1994), and Allen et al. (1995). This, in turn, would imply that the observed radial CO profile is the result of the distribution of the SF, rather than lying at the origin of the latter. This is an interesting idea that we cannot pursue further with the present data, but which warrants further research.

6   ORIGIN AND ROLE OF HI

The radial H I profile is perhaps the most challenging to our understanding of all profiles presented here. In contrast to all other tracers, a central peak is absent, corresponding to the central depression seen on an H I image of M100 (see Fig. 1 of the present paper; also Warmels 1988; Cayatte et al. 1990; Knapen et al. 1993). A central H I depression is not at all uncommon in barred galaxies (e.g. NGC 3992: Gottesman et al. 1984; NGC 1365: Ondrechen & van der Hulst 1989; Jörsäter & van Moorsel 1995), but some barred galaxies do contain H I in their central regions (e.g. NGC 5383: Sancisi, Allen & Sullivan 1979; NGC 4731: Gottesman et al 1984; NGC 1097: Ondrechen, van der Hulst & Hummel 1989). Of the 9 non-barred galaxies studied by Wevers, van der Kruit & Allen (1986), 5 show evidence for a central H I depression, whereas of the 6 galaxies classified as barred, 5 have a central depression. From the shape of the radial H I profiles, it is not possible to predict the classification of the galaxy as barred or non-barred. Broeils & van Woerden (1994) present radial H I profiles of 48 spiral galaxies, of which 14 are classified as barred. Some of the radial profiles derived show a depression in the central region, others do not, and while there is a trend with morphological type (with early-type spirals having more of a central H I depression), no systematic differences in behaviour can be seen between barred and non-barred galaxies. We thus conclude that the idea that bar dynamics cleans the bar region from H I by channeling the gas inward toward the nuclear zone and outward toward the "cusps" at the ends of the bar, can in no case be a general scenario. It is not solely the presence of a bar which determines whether or not the H I is depressed in the central regions. Note that in some of these cases a bar in a galaxy may only appear in NIR imaging and not in the optical, although it seems unlikely that few-kpc length bars can be present in a substantial fraction of galaxies which were not classified as SX or SB by e.g. de Vaucouleurs et al. (1991). Another note to make here is that a central depression in H I cannot in general be taken as proof of a lack of neutral gas. A centrally peaked CO profile, such as seen in NGC 4321, seems to be the standard, even for barred spirals with H I-poor central regions (e.g. Sandqvist et al. 1995; see also the review by Young & Scoville 1991). As we will argue below, a central atomic gas depression may well indicate changes in the equilibrium between H I and H_2.

The H I disc profile of NGC 4321 shows an interesting plateau of slightly enhanced emission, coinciding with the region of the SF spiral arms as defined in Hα. This indicates a relation between H I and SF activity, with either more SF occurring because of the enhanced atomic gas density, or more

H I present because of the SF activity. The first possibility is contradicted by the CO measurements, which indicate that molecular hydrogen is more abundant over the whole region, by more than an order of magnitude up to $R \sim 100''$ (Kenney & Young 1988; Cepa et al. 1992; Knapen et al. 1996). We should note that there are no definite indications so far that the CO to H$_2$ conversion factor X in NGC 4321 differs from the assumed "standard" value measured in the Galaxy (Rand 1995 found only weak, but inconclusive, evidence for a lower factor), but that even if there is a variation of order 2-3, as may well be the case in M51 (Adler et al. 1992; Rand 1993; Nakai & Kuno 1995), it is extremely improbable that the H I is more abundant than H$_2$ in most of the region considered here. Fig. 4 thus shows that H I is more abundant where SF is present, and its increased column density is almost certainly a result of the SF. The shape of the radial H I disc profile is very similar to the interarm profile (Fig. 6b), whereas the H I profile is almost completely flat in the arm regions (Fig. 6a).

A probable hypothesis for the origin of H I is its production by photodissociation of the molecular hydrogen by the UV radiation field of young massive stars. Allen, Atherton & Tilanus (1986) showed evidence for this in M83 from the displacement of gas and dust from massive star formation and H I (see also Tilanus & Allen 1989, 1991). Similar offsets between tracers were also observed in M51 (Vogel et al. 1988; Rand & Kulkarni 1990).

In M51, Knapen et al. (1992) and Rand et al. (1992) found that several peaks in Hα were accompanied by peaks in H I, and argued that the H I peaks were caused by the enhanced SF activity through photodissociation of molecular gas. Again, the atomic hydrogen is almost certainly not the cause of the star formation since the molecular hydrogen is an order of magnitude more abundant at the radii where the peaks occur.

In NGC 4321, evidence for the same process is seen using two separate observational methods. First, spatial correspondence is observed between H I and Hα, whereas both are clearly offset from the dust lanes (Sect. 3). The CO spiral arms are coincident with the dust lanes in the inner part of the disc (Rand 1995). This situation is very similar to that observed in M51 (see above), but the situation in the arm region just south of the centre is not clear (see Sect. 3.3), and more reminiscent of that in M83 (Lord & Kenney 1991). Second, radial profiles (Sect. 4) show that although the H I behaves very differently from other tracers, which are all directly related to SF (see before), it is enhanced in the region where the spiral arms are forming stars most actively.

The globally flat H I column density profile over a wide radial range in NGC 4321 is a feature relatively common in spirals. An explanation was given by Shaya & Federman (1987) who suggested that the H I column density observed corresponds to that required to shield from the ambient UV field the H$_2$ clouds of which the H I forms an evaporative envelope. They explained that the column density of the H I cloud around a molecular cloud with no embedded UV sources will not rise above the value required to self-shield the molecules against dissociation, due to the global UV field, since any further H I would then convert to H$_2$. We can add here that a similar consideration can be applied to clouds containing dust, provided that the dust to gas ratio does not vary dramatically within the disc. Once the

dust-shielding rises above a critical extinction value any additional H I converts to H$_2$. Savage et al. (1977) note, from measurements made within the Galaxy, that conversion to H$_2$ sets in for H I column densities of some 5×10^{20} cm^{-2}, corresponding to an $E(B-V)$ of 0.08, which in turn corresponds to a dust extinction at the dissociation edge for H$_2$ of ~ 0.7 mag. Thus the self-shielding explanation of Shaya and Federman must be supplemented by taking quantitatively into account the effects of dust, although the result is qualitatively similar.

We can see in Fig. 4 that the value of the H I column density over the radial range between 5 and 10 kpc, where it is virtually constant, is a little less than 5×10^{20} cm^{-2}. At total neutral hydrogen column densities significantly greater than this all the hydrogen converts to H$_2$, except in zones close to local UV sources within the clouds. This general tendency is seen as a decline in the H I column density at radii less than 5 kpc. Beyond 12 kpc the H I makes up all the neutral H, and the column density falls exponentially, as do the surface brightness indices. It is interesting to note that the arm H I column density in fact stays at its higher level up to ~ 15 kpc, as might be expected from the higher concentrations of SF, gas and dust there. The difference between our scenario and that of Shaya and Federman (1987), or the considerations of the physical processes involved in the H I to H$_2$ transition by Elmegreen (1993) is the extra effect of dust extinction which reduces the H I column required for shielding, and tends to enhance the H$_2$/H I ratio throughout the disc.

Whereas in the inner parts the H I may thus be partly produced by photodissociation of molecular gas by the radiation field from massive young stars, one cannot assume that the H I in the outer regions is completely independent of the local dissociating radiation field. Rand et al. (1992) find evidence from radial profiles of total gas, Hα and H I that dissociation by massive young stars still plays a role at large radii. But even if the massive stars are the most important source of photodissociating radiation, the correlation between Hα and H I may break down at large galactocentric radii. First, since the total densities of gas and dust are much lower than in the inner disc, photons can travel further from the stars that produce them, and molecular hydrogen can be dissociated at greater distances from the radiation sources, tending to weaken the small-scale H I–Hα correlation. Also, the metallicity may be so low in the outer regions of the disc that there are not enough dust-grains for molecular gas to form on. All these processes can lead to a more widespread distribution of H I. One example is the tidal arm of M51 observed in H I by Rots et al. (1990), where no Hα is detected. Some or all of the above-mentioned processes may cause the hydrogen in the arm to be predominantly atomic.

Although the Hα emission is used here to trace young massive stars, this is not entirely adequate for tracing the radiation field which photodissociates the molecular hydrogen and forms the H I. This radiation field will be more adequately observed in the far UV. An important line of future study will be the direct comparison between the tracers of the supposed origin (UV) and result (H I) of the photodissociation.

7   CONCLUSIONS

We have used images of the barred spiral galaxy NGC 4321 (M100) in optical (B and I bands), $B - I$ colour, Hα, H$\textsc{i}$, and 21cm radio continuum to study the geometrical distributions of gas and stars in and outside the spiral arms. We employ two main techniques. First, we overlay the different images to indicate the morphological relations between massive SF, atomic hydrogen gas, and dust lanes. Second, we study azimuthally averaged radial profiles for all tracers, comparing with CO data, for the whole disc, as well as the arm and interarm zones separately. Our main conclusions are the following:

(i) The dust lanes running along most of the spiral arms (and coinciding with the CO spiral arms in part of them; Rand 1995) are offset from the Hα arms and from the H$\textsc{i}$ arms which coincide spatially with Hα. This is very similar to the relations observed in some other spiral galaxies, and can be interpreted as an effect of the compression of gas by the density wave in the arm, with SF occurring downstream. H$\textsc{i}$ will be a *result* of the massive SF through photodissociation of part of the molecular gas by the UV radiation field (cf. Allen et al. 1986).

(ii) We observe a spatial coincidence of regions with enhanced Hα emission (i.e. with strong current massive SF) and with enhanced H$\textsc{i}$ density throughout the disc of the galaxy. Most probably the H$\textsc{i}$ in these regions has its origin in photodissociation by radiation from the nearby massive stars.

(iii) The radial profiles in Hα, blue and NIR light, radio continuum and also CO have equal (within the errors of the fit) exponential scale lengths in the region of the SF spiral arms. This is not only true for the complete disc, but also for the arm, and the interarm regions separately. The arm scale lengths are however longer (by $\sim 50\%$) than the disc and interarm scale lengths, which are comparable. These results indicate that the radial profiles are not influenced by dust extinction or radial gradients in stellar populations, which would lead to differences in the scale length values.

(iv) The equal disc, arm and interarm scale lengths in Hα, B, I and radio continuum indicate a common origin in star formation for these profiles. The fact that the CO disc profile has the same scale length would seem to indicate that the average efficiency of massive SF does not vary radially in the disc. The CO intensity could however be proportional to the cosmic ray density as indicated by the radio continuum profile, in which case the CO intensity would not be a linear indicator of the density of molecular gas.

(v) The H$\textsc{i}$ radial profile is quite different from the Hα, optical, radio continuum, and CO profiles. After a depression in the central region (which is not in general confined to barred spirals and cannot be explained by bar dynamical processes for re-distribution of gas alone) the profile rises in the region of the SF spiral arms, and is practically flat in that region. The rise is naturally explained by the photodissociation process, which should enhance the H$\textsc{i}$ density in the region of enhanced SF. The flatness of the profile in the disc is understandable at least qualitatively in terms of the equilibrium between atomic and molecular hydrogen in the presence of dust and SF.

REFERENCES

Adler, D.S., Allen, R.J., & Lo, K.Y. 1991, ApJ 382, 475
Adler, D.S., Lo, K.Y., Wright, M.C.H., Rydbeck, G., Plante, R.L., & Allen, R.J. 1992, ApJ 392, 497
Allen, R.J. 1992, ApJ 399, 573
Allen, R.J., Atherton, P.D., & Tilanus, R.P.J. 1986, Nature, 319, 296
Allen, R.J., Le Bourlot, J., Lequeux, J., Pineau des Forêts, G., & Roueff, E. 1995, ApJ 444, 157
Athanassoula, E. 1992, MNRAS 259, 345
Beckman, J.E., Peletier, R.F., Knapen, J.H., Corradi, R.L.M., & Gentet, L.J. 1996, ApJ, in press
Broeils, A.H., & van Woerden, H. 1994, A&AS 107, 129
Carignan, C. 1985, ApJS 58, 107
Cayatte, V., van Gorkom, J.H., Balkowski, C., & Kotanyi, C.G. 1990, AJ 100, 604
Cepa, J. & Beckman, J.E. 1990, ApJ 349, 497
Cepa, J., Beckman, J.E., Knapen, J.H., Nakai, N. & Kuno, N. 1992, AJ 103, 429
DeGioia-Eastwood, K., Grasdalen, G.L., Strom, S.E., & Strom, K.M. 1984, ApJ 278, 564
de Jong, R.S. 1995, PhD thesis, University of Groningen
de Vaucouleurs, G., de Vaucouleurs, A., Corwin, H.G., Buta, R.J., Paturel, G., Fouqué, P., 1991, Third Reference Catalogue of Bright Galaxies (RC3), Springer, New York
Elmegreen, B.G. 1993, ApJ 411, 170
Elmegreen, D.M. & Elmegreen, B.G. 1984, ApJS 54, 127
Evans, R., 1994, MNRAS 266, 511
Freedman, W. *et al.* 1994, Nature 371, 757
García-Burillo, S., Guélin, M., & Cernicharo, J. 1993, A&A 274, 123
Gottesman, S.T., Ball, R., Hunter, J.H., & Huntley, J.M. 1984, ApJ 286, 471
Grosbøl, P.J. 1985, A&AS 60, 261
Helou, G., & Bicay, M.D. 1993, ApJ 415, 93
Jörsäter, S., & van Moorsel, G.A. 1995, AJ, 110, 2037
Kenney, J.D. & Young, J.S. 1988, ApJS 66, 261
Knapen, J.H. 1996, in preparation
Knapen, J.H., & van der Kruit, P.C. 1991, A&A 248, 57
Knapen, J.H., Beckman, J.E., Cepa, J., van der Hulst, J.M. & Rand, R.J. 1992, ApJL 385, L37
Knapen, J.H., Cepa, J., Beckman, J.E., del Rio, M.S. & Pedlar, A. 1993, ApJ 416, 563
Knapen, J.H., Beckman, J.E., Shlosman, I., Peletier, R.F., Heller, C.H. & de Jong, R.S. 1995a, ApJL 443, L73
Knapen, J.H., Beckman, J.E., Heller, C.H., Shlosman, I. & de Jong, R.S. 1995b, ApJ 454, 623
Knapen, J.H., Beckman, J.E., Cepa, J. & Nakai, N. 1996, A&A, 308, 27
Lequeux, J., Le Bourlot, J., Pineau des Forêts, G., Roueff, E., Boulanger, F., & Rubio, M. 1994, A&A 292, 371
Lord, S.D., & Young, J.S. 1990, ApJ 356, 135
Lord, S.D., & Kenney, J.D.P. 1991, ApJ 381, 130
Nakai, N., Kuno, N., Handa, T., & Sofue, Y. 1991, in *Dynamics of Galaxies & their Molecular Cloud Distributions*, Eds. F. Combes & F. Casoli, Kluwer, Dordrecht, p.63
Nakai, N., Kuno, N., Handa, T., & Sofue, Y. 1994, PASJ 46, 527
Nakai, N., & Kuno, N. 1995, PASJ 47, 761
Ondrechen, M.P., & van der Hulst, J.M. 1989, ApJ 342, 29
Ondrechen, M.P., van der Hulst, J.M., & Hummel, E. 1989, ApJ 342, 39

Peletier, R.F. 1994, Spectrum Newsletter 3, 28

Peletier, R.F., Valentijn, E.A., Moorwood, A.F.M., Freudling, W., Knapen, J.H., & Beckman, J.E. 1995, A&A, 300, L1

Pierce, M.J. 1986, AJ 92, 285

Rand, R.J. 1993, ApJ 404, 593

Rand, R.J. 1995, AJ 109, 2444

Rand, R.J., & Kulkarni, S.R. 1990, ApJ 349, L43

Rand, R.J., Kulkarni, S.R., & Rice, W. 1992, ApJ 390, 66

Regan, M.W., Vogel, S.N. 1994, ApJ 434, 536

Regan, M.W., Vogel, S.N. 1995, ApJ 452, L21

Rots, A.H., Crane, P.C., Bosma, A., Athanassoula, E., van der Hulst, J.M. 1990, AJ 100, 387

Rubio, M., Lequeux, J., & Boulanger, F. 1993, A&A 271, 9

Ryder, S.D. & Dopita, M.A. 1994, ApJ 430, 142

Sandqvist, Aa., Jörsäter, S., & Lindblad, P.O. 1995, A&A 295, 585

Sancisi, R., Allen, R.J., & Sullivan, W.T. 1979, A&A 78, 217

Savage, B.B., Bohlin, R.C., Drake, J.F. & Budich, W. 1977, ApJ 216, 291

Schweizer, F. 1976, ApJS 31, 313

Shaya, E.J. & Federman, S.R. 1987, ApJ 319, 76

Tacconi, L.J., & Young, J.S. 1986, ApJ 308, 600

Tacconi, L.J., & Young, J.S. 1990, ApJ 352, 595

Tilanus, R.P.J., Allen, R.J., van der Hulst, J.M., Crane, P.C., & Kennicutt, R.C. 1988, ApJ 330, 667

Tilanus, R.P.J., & Allen, R.J. 1989, ApJ, 339, L57

Tilanus, R.P.J., & Allen, R.J. 1991, A&A, 244, 8

Vogel, S.N., Kulkarni, S.R., & Scoville, N.Z. 1988, Nature 334, 402

Warmels, R.H. 1988, A&AS 72, 19

Wevers, B.M.H.R., van der Kruit, P.C., & Allen, R.J. 1986, A&AS 66, 505

Young, J.S., & Scoville, N.Z. 1982, ApJ 258, 467

Young, J.S., & Scoville, N.Z. 1991, ARA&A, 29, 581